Manipulation of *in Vitro* Angiogenesis Using Peptide-Coated Gold Nanoparticles

Dorota Bartczak,[†] Otto L. Muskens,[†] Tilman Sanchez-Elsner,[‡] Antonios G. Kanaras,[†,*] and Timothy M. Millar[‡,*]

[†]Institute for Life Sciences, Physics and Astronomy, Faculty of Physical Sciences and Engineering, University of Southampton, SO17 1BJ, U.K. and [‡]Faculty of Medicine, Southampton General Hospital, University of Southampton, Southampton, SO17 1BJ, U.K.

ABSTRACT We demonstrate the deliberate activation or inhibition of *in vitro* angiogenesis using functional peptide coated gold nanoparticles. The peptides, anchored to oligo-ethylene glycol capped gold nanospheres, were designed to selectively interact with cell receptors responsible for activation or inhibition of angiogenesis. The functional particles are shown to influence significantly the extent and morphology of vascular structures, without causing toxicity. Mechanistic studies show that the nanoparticles have the ability to alter the balance between naturally secreted pro- and anti-angiogenic factors, under various biological conditions. Nanoparticle-induced control over angiogenesis opens up new directions in targeted drug delivery and therapy.

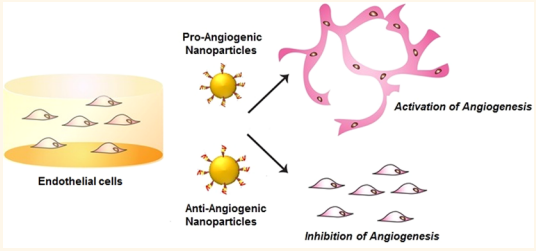

KEYWORDS: gold nanoparticles · angiogenesis · peptides · tumors · pro-angiogenic · anti-angiogenic · drugs

Angiogenesis is a process where new blood vessels are formed in order to deliver oxygen and nutrients throughout the body.[1] Thus, angiogenesis is vital in growth and development, playing a pivotal role in wound healing, pregnancy, rheumatoid disease, cardiovascular processes, eye diseases, and importantly the growth and metastasis of tumors.[2−4] Angiogenesis starts when endothelial cells are activated by specific molecules that bind to angiogenic receptors, promoting a signaling cascade. This activation results in the proliferation of endothelial cells, which then assemble to form the new vascular structures. The process is under strict control of signals that regulate the growth of new vessels by activation (pro-angiogenic factors) or inhibition (anti-angiogenic factors), when necessary. Pathological angiogenesis derives from disruptions in the fragile balance between stimulating and inhibiting factors.[5,6] Due to the high importance of this process, there is intense research activity aimed at the discovery of angiogenic drugs (often small organic molecules, proteins, or antibodies) that can increase or deplete the growth of capillaries.[7] However, although sometimes temporarily effective, in many cases these drugs must be introduced in large quantities, which could lead to nonspecific binding, unexpected toxicities, and undesired side effects.[8]

Nanoparticulate systems can offer an alternative way to target angiogenesis.[9−12] One of their great advantages is the requirement for low doses due to their increased reactivity that derives from the large concentration of active molecules confined in the small volume of a nanoparticle. Furthermore, the versatility of chemical strategies to modify their surface allows the immobilization of several molecules, offering a multifunctional ability.[13−17] Among several kinds of particles with various chemical compositions,[18] the utilization of simple types of inorganic nanoparticles (*i.e.*, gold) offers additional benefits in imaging and therapy, deriving from the optical and thermal properties of the metal core.[19−24]

A limited number of studies so far has addressed the development of inorganic nanoparticles with pro-angiogenic and anti-angiogenic properties.[25,26] Mukhopadhyay and co-workers reported that europium hydroxide nanorods can promote proliferation

* Address correspondence to a.kanaras@soton.ac.uk, t.m.millar@soton.ac.uk.

Received for review April 27, 2013 and accepted May 23, 2013.

Published online May 28, 2013
10.1021/nn402111z

and vascular sprouting of endothelial cells in a dose-dependent manner. The governing mechanism was found to be an increase in the production of the reactive oxygen species (ROS) deriving from the chemical composition of the nanorods.[27,28] The same group showed that "naked" 5 nm gold nanoparticles, *i.e.*, without an organic capping layer, interact selectively with a heparin-binding growth factor (through sulfur/amines existing in the heparin-binding domain) and inhibit angiogenesis.[29,30] Recently, Mukherjee and co-workers demonstrated that the anti-angiogenic property of bare gold nanoparticles is lost when the particles are covered with nonfunctional charged ligands.[31]

In earlier work, we investigated several types of interactions between endothelial cells (ECs), the building units of angiogenesis, and three chosen types of peptide-coated nanoparticles:[32−35] P1 (KPQPRPLS), which binds to the vascular endothelial growth factor receptor (VEGFR-1) and promotes signal cascade activating angiogenic genes; P3 (KATWLPPR), which predominately binds to neuropilin-1 receptor (NRP-1) and promotes receptor internalization; and P2 (KPRQPSLP), which does not interact with any of these receptors and is simply taken up by the cells.

Here, we expand this work employing the three types of peptide-coated nanoparticles in *in vitro* angiogenesis, presenting for the first time control of the activation or inhibition of blood vessel growth. Mechanistic studies reveal how the functional nanoparticles influence the process of angiogenesis. We believe that these studies are critically important to the understanding of the interactions between the chosen nanoparticles and angiogenesis and will open up new directions in angiogenic treatments using gold nanoparticles as a platform for drug development.

RESULTS AND DISCUSSION

Gold nanoparticles (NPs) with a narrow size distribution (15 ± 2 nm) were synthesized following the Turkevich method.[36] To ensure robustness and biocompatibility, the particles were capped with monocarboxy (1-mercaptoundec-11-yl) hexakis(ethylene glycol) (OEG) as reported elsewhere.[37] The OEG-NPs were functionalized with the three peptides (P1, P2, P3) following previous protocols established in our group.[38] Initially the endothelial cells were placed in a matrix gel under reduced serum conditions. Then, their growth into vascular structures was monitored at different time intervals (2, 4, and 8 h) in the presence of the three different types of gold nanoparticles: the "activators" (P1-OEG-NPs), the "inhibitors" (P3-OEG-NPs), and the "mutants" (P2-OEG-NPs).

Activation and Inhibition of Angiogenesis. Figure 1a shows phase contrast images of the angiogenic process at various incubation times. As can be seen, the samples containing only endothelial cells show neovascular sprouting after 8 h of incubation. This is not unexpected and results from the residual growth factors contained in the matrix gel. A similar observation is made for the samples containing the mutant particles, allowing us to safely assume that this type of particle does not influence the rate of the angiogenic process (see Figure S3). On the other hand, the observations for the samples where the activators and inhibitors were introduced are substantially different. For the matrix gel containing the activators, capillary formation is easily observed even after 2 h of incubation, while the sample containing the inhibitors does not show any sign of angiogenesis (even after 8 h hours of incubation).

Further quantification of these general observations was done by statistical image analysis using the mathematical algorithm AngioQuant (v1.33).[39] Computer-assisted analysis allows recognition of the main vascular network by conversion of the microscopy image to a skeleton (see Figure S2). Three parameters were extracted for each image: the total vessel length, the fractional area coverage of the cells/capillaries (taking into account their width), and the number of junctions in the skeleton network. Results are shown in Figure 1b for the activators and inhibitors compared to untreated endothelial cells. The quantitative analysis confirms the trend shown in the images, namely, that the activator nanoparticle−peptide complex significantly accelerates angiogenesis. This effect is especially pronounced during the first hours of incubation, where the P1-activated capillary network is almost fully developed after 4 h. The growth saturates when the vascular network reaches coverage of around 25%. The image analysis reveals that after 8 h the morphology of the vascular structures activated by the P1-OEG NPs is equivalent to those generated at a slower rate by the growth factors found in the matrix gel. Thus, the activation of endothelial cells with P1-functionalized NPs produces a considerable (factor of 2) acceleration of angiogenesis without resulting in significant morphological differences compared to neovascular sprouting caused naturally by the matrix gel.

The sample containing the inhibitors shows a marked anti-angiogenic effect in Figure 1b. All three parameters (vessel length, fractional area, and number of junctions) are drastically compromised for times longer than 2 h after treatment. A comparison with the samples containing only endothelial cells (Figure 1b) or endothelial cells with the mutant particles (see Figure S3) led us to attribute the anti-angiogenic effects to the functionality of the nanoparticle−peptide complex alone. Indeed, in our experiments the gold core is not naked but coated with OEG and peptides, which prevents the nonspecific binding of any growth factors, as in the case of Mukhopadhyay and co-workers.[29,30]

Mechanistic Studies. During angiogenesis, the endothelium undergoes structural changes, including loss of barrier function, leading to an increased permeability of the endothelial monolayer. To assess the degree of

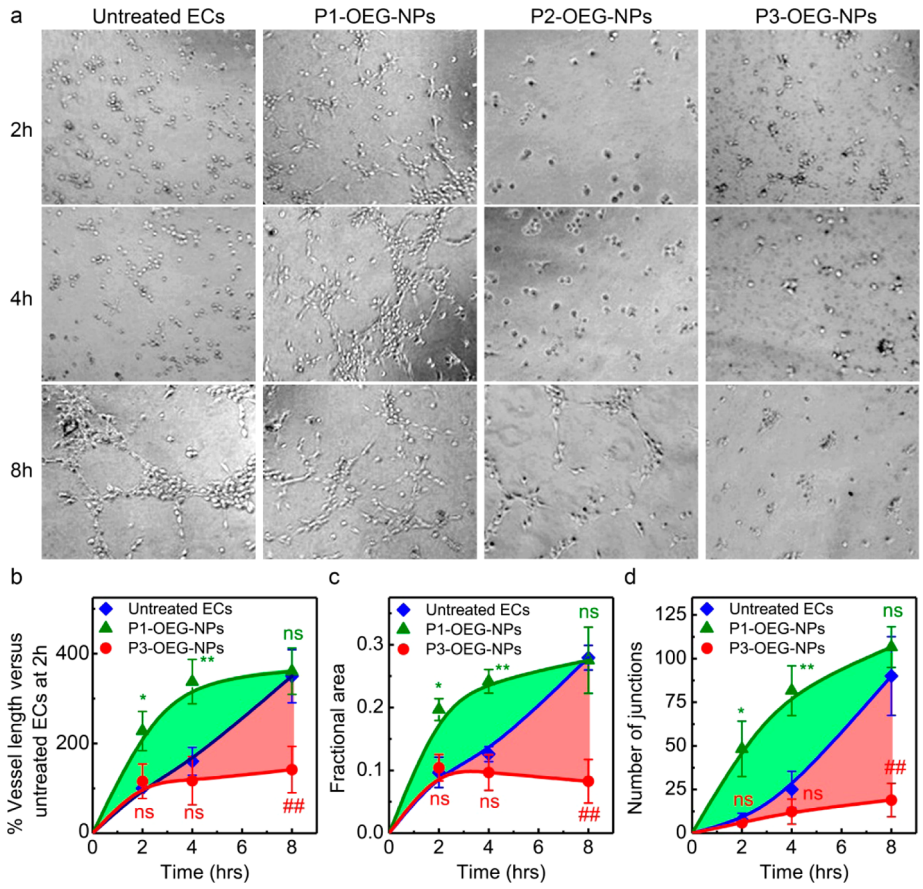

Figure 1. Peptide-coated gold nanoparticles activate or inhibit angiogenesis. (a) Phase contrast images show endothelial cells grown on reduced serum matrix gel after treatment with P1-OEG-NPs (activators), P2-OEG-NPs (mutants), or P3-OEG-NPs (inhibitors) or nontreated with particles (untreated ECs) and for 2, 4, and 8 h after incubation. (b–d) Results from computer-assisted quantitative analysis of angiogenesis showing total vessel length (b), fractional area coverage (c), and number of junctions (d); *$p \leq 0.05$, **$p \leq 0.01$, ***$p \leq 0.001$ significance *versus* control time points; $^{\#\#}p \leq 0.01$ significance decrease *versus* control time points; ns nonsignificant *versus* control ($n = 3$, mean ± SD). For clarity P2-OEG-NPs *versus* control is shown in Figure S2.

permeability caused by the different types of nanoparticles, we performed the following experiment. A confluent layer of endothelial cells was treated with the different types of nanoparticles for 24 h, and then the permeability of the monolayer was examined by the diffusion of a fluorescently labeled high molecular weight (40 kDa) dextran through the layer.

Figure 2a shows the results of the assay. As can be seen, a 24 h stimulation with the activators caused an increased permeability beyond the level expected by an ordinary endothelial cell monolayer (see bar marked "untreated"). In agreement with our previously reported findings,[32−35] a high permeability typically occurs after growth factor receptor binding, and it is considered the first stage in the process of angiogenesis. Surprisingly, when the assay was applied in the presence of the inhibitors, it also led to increased cell monolayer permeability (compared to untreated cells and cells incubated with mutants). Since the P3 peptide, attached to the inhibitors, interacts with the NRP-1 receptor, we hypothesize that the permeability is related to the reported role of NRP-1 in cell adhesiveness *via* integrin regulation.[40,41] In order to verify our hypothesis, we used an assay to measure the number of adherent cells after 24 h treatment with the different types of nanoparticles. The results in Figure 2b show that a significant number of cells were detached when they were incubated with the inhibitors (see also Figure S4). This observation suggests that NRP-1 signaling, an important function of the receptor in the regulation of the angiogenic process, is related to monolayer permeability. Conversely, the cultures with activators and mutants did not show any change in the number of adherent cells, which (i) correlates with the lack of a receptor signaling caused by mutants, leading to permeability changes, and (ii) confirms that the pro-angiogenic effects of the activators causes a change in permeability *via* changes in cell-to-cell contact rather than by the acute loss of cells.

Endothelial cells are an adhesive cell type where the loss of adhesion could be correlated to cytotoxicity as cells progress through cell death and apoptosis. Therefore, an alternate explanation for a reduced cell adhesion in the sample that contains the inhibitors

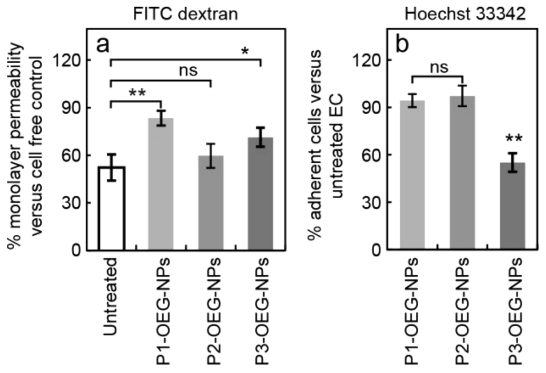

Figure 2. Peptide-functionalized NPs cause changes in EC barrier function and cellular adhesion. (a) Endothelial cell monolayer permeability, evaluated 24 h after treatment with different types of peptide-coated nanoparticles. The results are compared to untreated endothelial cell monolayer. The assay is based on the transportation of fluorescein isothiocyanate–dextran (FITC dextran) through a confluent cell monolayer grown on polyethylene terephthalate (PET) membrane trans-wells with a 0.4 μm pore size. Signals are normalized to the background fluorescence from the cells. (b) Percentage of adherent cells quantified through the total DNA labeled with the dye Hoechst 33342 by measuring relative fluorescence normalized to untreated EC monolayer; *$p \leq 0.05$, **$p \leq 0.01$, ***$p \leq 0.001$, ns nonsignificant ($n = 3$, mean $\pm$ SD).

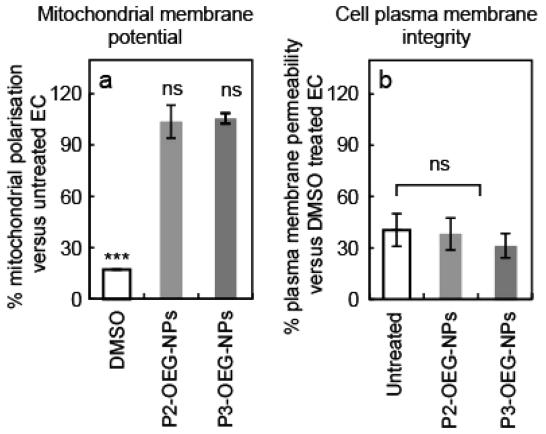

Figure 3. Peptide-functionalized NPs show no significant changes on mitochondrial membrane polarization and cell plasma membrane integrity of ECs. Mitochondrial membrane potential (a) and cell plasma membrane integrity (b) measured by flow cytometry following 24 h treatment with inhibitors and mutants using the JC-1 and PI fluorescent assays, respectively; *$p \leq 0.05$, **$p \leq 0.01$, ***$p \leq 0.001$, ns nonsignificant ($n = 3$, mean $\pm$ SD). In (a) DMSO is used as a negative control that disrupts the potential of the mitochondrial membrane. In (b) the results for the mutants and the inhibitors are normalized to permeability caused by DMSO and compared to untreated cells, showing no significant changes in the cell plasma membrane integrity.

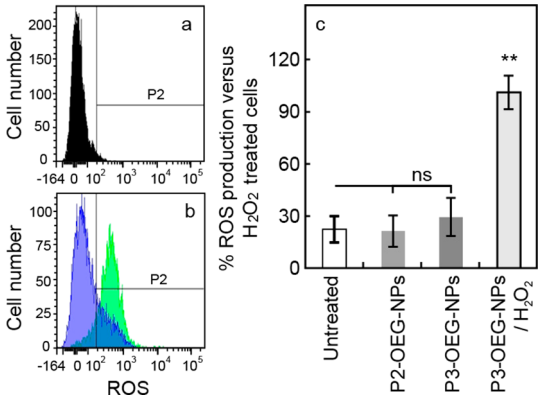

Figure 4. Production of free radicals (ROS) in the presence of inhibitor nanoparticles against mutant particles and untreated cells. ROS histograms for untreated cells alone (black) (a) and for P3-OEG-NPs treated (blue) or P3-OEG-NPs in the presence of H_2O_2 (green) (b). P2 refers to the gating strategy in (a) and (b). Resulting average ROS production for untreated ECs and for ECs incubated with peptide–NP complexes, normalized to ECs treated with H_2O_2 (c). The dye carboxy-DFFDA was used in the assay. P3-OEG-NPs/H_2O_2 is employed as positive control. *$p \leq 0.05$, **$p \leq 0.01$, ***$p \leq 0.001$, ns nonsignificant ($n = 3$, mean $\pm$ SD).

might be associated with the potential cytotoxicity caused by the gold nanoparticles. To rule out this hypothesis, we assessed the cytotoxicity of the inhibitor nanoparticles. There are multiple aspects and possible cytotoxic effects of NPs on cells, and a variety of assays can be utilized to assess potential damage. Mitochondrial membrane potential and plasma membrane integrity are early and late markers of cytotoxicity and apoptosis, respectively. Figure 3 shows that no significant changes were observed in mitochondrial membrane potential and cell plasma membrane integrity when combined populations of floating and adherent cells were examined. This indicates that association of cells with NPs does not put cells under cytotoxic stress. Additionally, reactive oxygen species are naturally occurring signaling molecules, which have also been shown to increase during times of cellular stress, leading to cytotoxicity. Figure 4 shows the monitoring of ROS levels in the presence of mutants and inhibitors. An assay based on the dye carboxy-DFFDA shows that no significant ROS levels are detected in the samples. Thus, NP-mediated inhibition of angiogenesis is purely derived from the selective receptor binding rather than any inherent cytotoxicity.

Inhibition of Angiogenesis Caused by Cancer Cell Media. In the above experiments we demonstrated that peptide-functionalized gold nanoparticles can be used to deliberately influence the functionality of endothelial cells in the angiogenic process in a relatively simple model system. In order to develop nanoparticulate platforms that can successfully trigger or inhibit angiogenesis through selective binding to the relevant receptors, one has to address another, even more important question: how does the nanoparticulate platform behave in tumor angiogenesis? In tumor angiogenesis, the surrounding environment is more complex, as the tumor itself also secretes angiogenic factors and promotes angiogenesis. Cancerous environments actively accelerate vascularization in order to obtain sufficient oxygen and nutrients for growth and metastasis. The first question to be answered toward

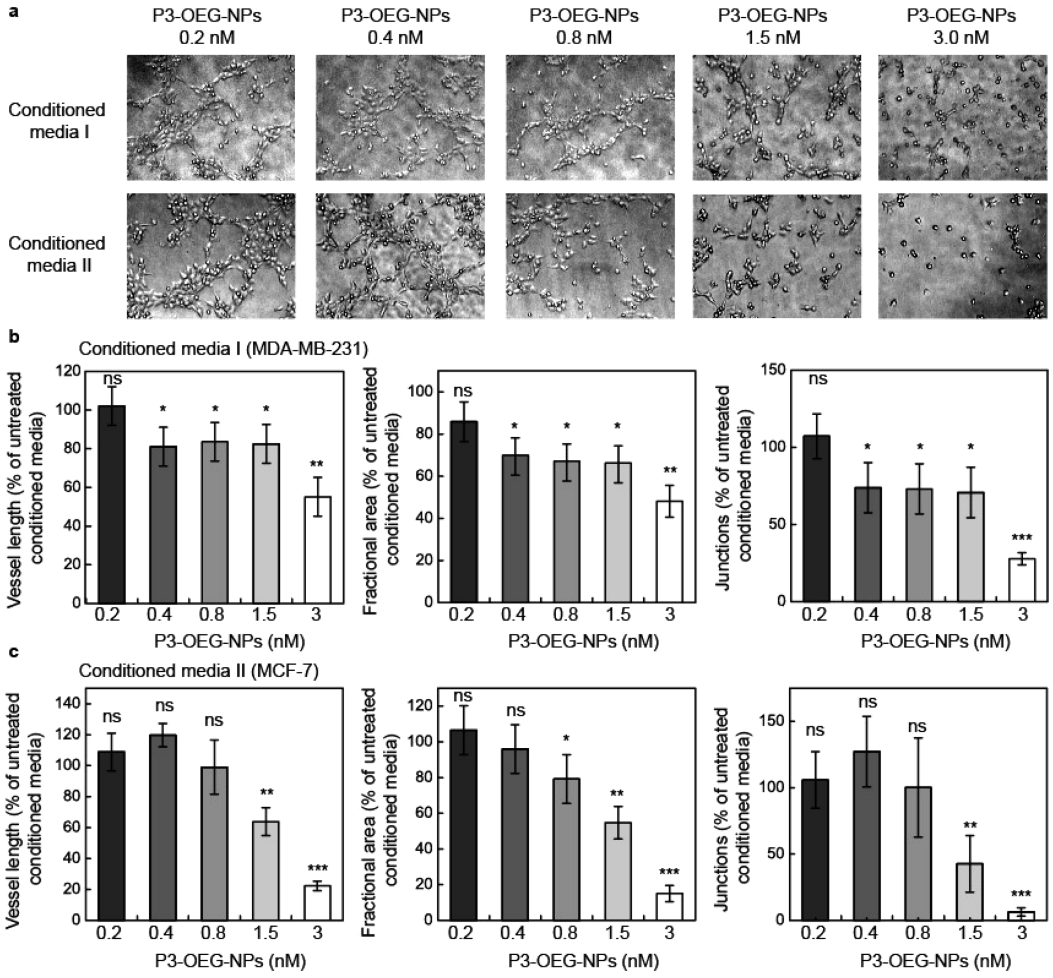

Figure 5. Cancer cell conditioned media causes angiogenesis, which can be blocked by pretreatment of cancer cells with a sufficient concentration of inhibitors. Phase contrast images of ECs on matrix gel after 8 h treatment with conditioned media, derived from 24 h treatment of MDA-MB-231 cells (media I) or MCF-7 cells (media II) exposed to inhibitor nanoparticles at different doses (0.2−3 nM). The graphs represent quantitative analysis of microscope images covering an area of 800 × 600 μm^2, of the overall length, area fraction, and number of junctions of capillaries formed following treatment of ECs with cancer cell conditioned media (100%), compared to conditioned medium from cancer cells without nanoparticles. *$p \leq 0.05$, **$p \leq 0.01$, ***$p \leq 0.001$, ns nonsignificant.

this direction is if our activators or inhibitors interact directly with common tumors. For these experiments, we selected two human breast cancer cell lines (MCF-7 and MDA-MB-231), which were derived from metastatic breast cancers localized to the lung and which have been shown previously to release angiogenic factors.[42] We employed previously developed protocols[35] to tag nanoparticles with the dye HiLyte and used these particles to assess their interactions with cancerous cell lines by flow cytometry. Figure S5 shows that particles interact with the cancer cells but less so in comparison to endothelial cells.

There remains the intriguing possibility that the interaction of our inhibitor nanoparticles with cancer cells may either alter the cells ability to release angiogenic factors or reduce their capacity to adhere to the substrate (as seen for endothelial cells). To address this, we performed an experiment where we monitored the effectiveness of cancer cells to drive angiogenesis *via* released angiogenic factors following exposure to different doses of P3-OEG-NPs.

In this experiment, cancer cells were exposed to the inhibitors for 24 h. Subsequently the medium, following removal of cells, debris, and P3-OEG-NPs by centrifugation, was added to endothelial cells on a gel matrix. First, the amount of growth factors required for activating angiogenesis was optimized by calibrating the neovascular sprouting for samples with an increasing number of cancer cells (Figure S6). A concentration of 50 000 cancer cells per 200 μL was found to produce sufficient growth factors and was used in the subsequent experiments. Figure 5 shows the relevant phase contrast images of ECs on the gel matrix after 8 h treatment with the conditioned media obtained from cancer cells exposed to different doses of P3-OEG-NPs. As can be seen, angiogenesis mediated by cancer cell conditioned media was suppressed when the cancer cells had been incubated with the inhibitors

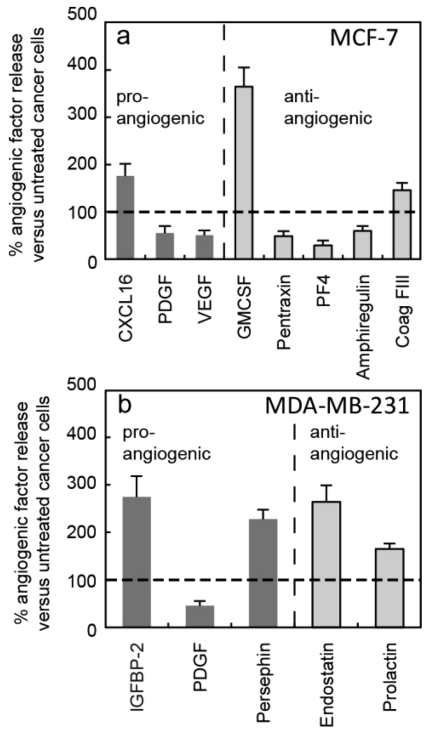

Figure 6. Effect of P3-OEG-NP inhibitors on pro-angiogenic (dark bars) and anti-angiogenic (gray bars) factors released by the cancer cells. Cancer cells were treated for 24 h with particles, and a range of angiogenic factors in the media was identified deriving from the different cancer lines (a) for MCF-7 and (b) for MDA. Dotted line at 100% is the level of protein released in nonstimulated cells and is used to calculate the relative level of released protein following treatment. All protein levels shown in the figure are significantly increased or decreased compared to control (n = 3, mean ± SD). For a more detailed profile see Figure S7 in the Supporting Information.

in a concentration-dependent manner. These observations indicate a change in the release of pro-angiogenic factors *via* a direct effect on cancer cells, potentially through changes in the release of angiogenic factors mediated by NPR-1 stimulation/blockade.

To further investigate the direct effect of P3-OEG-NPs on the release of angiogenic factors by cancer cells, we used a protein array targeted at both pro- and anti-angiogenic factors to measure the levels of factors released from cultures of the cancer cell lines over 24 h in the presence or absence of inhibitors. The level of proteins in the conditioned cultured media were compared to levels in cell-conditioned media from untreated cells, which constituted the 100% control levels. Figure 6 shows that inhibitors not only reduce the levels of a range of pro-angiogenic factors but also increase several anti-angiogenic factors (see Figure S7 for the full angiogenic profile). Although the specific role of each protein in this complex milieu is difficult to define, it is likely to be the overall balance between pro- and anti-angiogenic factors, which leads to the inhibition of angiogenesis shown in Figure 5. Therefore, the inhibitor nanoparticulate platform that we have developed possesses a unique ability to selectively regulate angiogenesis *via* dual modes of action. The particles (i) inhibit endothelial cell capillary formation by binding to NRP-1 receptors expressed by these cells and (ii) selectively alter the secretion of pro- and anti-angiogenic factors produced by cancer cells, reducing the possibility of cancer lead neovascularization and metastasis.

CONCLUSION

In conclusion, we demonstrated the manipulation of *in vitro* angiogenesis using peptide-coated gold nanospheres. Depending on the peptide function, the NPs (activators or inhibitors) promoted or blocked the capillary formation by ECs without causing toxicity to the cells, and both activators and inhibitors caused barrier dysfunction following different mechanisms. The treatment with activators accelerated neovascularization by a factor of 2 compared to untreated endothelial cells. Stimulation of angiogenesis is of interest for biomedical applications where promotion of vascular growth is desirable (*i.e.*, wound healing). On the other hand, we demonstrated that the inhibitors can selectively inhibit angiogenesis. This happens (a) *via* a receptor-mediated function by binding to angiogenic receptors on endothelial cells and (b) by changing cancer cell secretion of pro- and anti-angiogenic factors. We believe that the results presented in this paper will open up new directions for the development of angiogenic drugs based on inorganic nanoparticulate systems. The great advantage of this type of particle is that they can offer new routes of targeted delivery using multifunctional coatings and may allow additional advantages for imaging and treatment based on the properties of their inorganic core. Future studies will explore the potential of these new types of nanoparticle–peptide complexes in biomedical applications, such as wound healing or the treatment of cancer.

EXPERIMENTAL METHODS

Preparation of Peptide OEG Coated Nanoparticles. Sodium citrate stabilized spherical gold nanoparticles were prepared *via* the citrate reduction method[36] and functionalized with OEG. P1, P2, and P3 peptides were conjugated to OEG-coated nanoparticles using coupling agents. All of these procedures as well as characterization of the peptide-coated nanoparticles are described in detail in previous publications and in the Supporting Information.[32−35]

Isolation of Human Endothelial Cells. Human umbilical vein endothelial cells were isolated as described previously.[32−35] Briefly, umbilical cords were collected and cannulized before the addition of Type I collagenase solution (1 mg/mL) (Worthington), which was added to remove endothelial cells from the surface of the vessel wall. Following centrifugation, cells were cultured on gelatin-coated tissue culture flasks until confluence in 20% human serum, M199 media (Gibco), and Pen/Strep/Glut at 37 °C in humidified 5% CO_2 balanced air.

All experiments were carried out with cells at passage one, and endothelial lineage was shown by CD31 and von Willebrand Factor expression.

***In Vitro* Angiogenesis.** The experiments for the different conditions were adopted to protocols supplied by the manufacturers (Geltrex, Gibco, and μ-Slide Angiogenesis, ibiTreat). Briefly, 10 μL of gel, 10.000 EC, 40 ng of VEGF-B167, 2 ng of peptides (P1 or P2, MW = 922.1; P3, MW = 968.2), 4 fmol of peptide-coated nanoparticles, and 2.5% HS M199 media were used per well for different experiments. For the case of tumor angiogenesis, the serum-free M199 media was collected after 24 h culture of MDA-MB-231 or MCF-7 (50 000 cells per 200 μL) with or without inhibitor nanoparticles (3 nM). Afterward, it was centrifuged for 15 min, at 16 400 rpm, to precipitate out any cells and NPs, then mixed (1:1) with 5% HS M199 before use. The assay duration was varied between 2 and 24 h from seeding. Phase contrast images of live capillary-like structures were taken with an IX81 Olympus microscope and then analyzed by measuring the overall length of capillaries per image, number of junctions, and fractional area using AngioQuant (v1.33) quantification software.

EC Monolayer Permeability. To determine the effects of the peptides on endothelial barrier function and permeability, the ability of cell monolayers to prevent large molecules from passing through the barrier layer was probed. In detail, a confluent monolayer of EC, grown on gelatin-coated (0.2% porcine skin, Sigma) polyethylene terephthalate (PET) culture inserts (12-well microplate, BD Biosciences), was treated with peptide-coated nanoparticles (1.3 mL, 2.3 nM) in 20% HS M199 media for 24 h. After treatment, the media was aspirated, and cells were washed twice with HBSS before the addition of FITC-dextran (MW = 40 000 Da, 300 μL, 10 mg/mL, HBSS) to the monolayer along with additional HBSS (1 mL) that was placed in the well under the insert. After 7 min the inserts were removed and the quantity of FITC-dextran, which leaked through the cell monolayer, was measured with an Ascent Fluoroscan plate reader (Labsystems), at 485 nm excitation and 527 nm emission wavelengths. The results are expressed as a percentage of FITC-dextran passing through a PET membrane in the absence of cells (100% permeability) and in the absence of FITC dextran (0% permeability).

Number of Adherent Cells. Angiogenesis requires a change in the adhesive processes of cells, and the effect of the peptide nanoparticle treatments on cell number was measured. There is also a potential toxicity effect of the treatments, and the calculation of cell number is the first step in assessing this potential. Using the relative amounts of DNA as a surrogate for cell number, we were able to assess the effects of treatments. One-hundred percent confluent (EC) monolayers and 80% confluent breast cancer cells (96-well microplate) were treated with the inhibitors (200 μL/well, 3−0.02 nM) or DMSO (10%) in 20% HS M199 media (EC) or 10% HS DMEM (MDA and MCF-7) for 24 h. After treatment media was aspirated and cell nuclei were stained with Hoechst (1 μg/100 μL/well) in HBSS for 15 min in the dark. Then, it was washed twice prior to measurements (HBSS, 200 μL/well) with an Ascent Fluoroscan plate reader (Labsystems) at 355 nm excitation and 460 nm emission wavelengths. The intensity of the fluorescence signal is proportional to the number of adherent cells ($r^2 = 0.98 \pm 0.03$, $n = 10$) that remained after treatment. Results are presented as a percentage of stained untreated cells (100%) compared to unstained untreated controls (0%).

Mitochondrial Membrane Potential. One of the first markers of toxicity and cell death is the depolarization of mitochondrial membranes. Using the polarization-specific dye 5,5′,6,6′-tetrachloro-1,1′,3,3′-tetraethylbenzimidazole-carbocyanine iodide (JC-1), which fluoresces red in polarized mitochondrial membranes and green on depolarization, it is possible to determine the effects of treatments on cell viability. ECs (100 000) seeded on a 12-well microplate were treated with the different peptide-coated nanoparticles (1 mL, 3 nM), DMSO (10%), or methanol (MeOH, 20%) in 20% HS M199 media for 24 h. The JC-1 stain (10 μL, 500 μg/mL, HBSS) was then added, and cells were incubated for an additional 30 min. After incubation, the media was transferred into tubes and cells were harvested from the culture dish with trypsin/EDTA solution (0.5 mL, Sigma-Aldrich) for 5 min. The harvested cell suspensions were combined with collected media and centrifuged for 5 min at 1500 rpm. Cell pellets were resuspended in HBSS (0.2 mL) prior to measurements by flow cytometry (FACSCalibur, BD Biosciences) using 488 nm excitation wavelength with FL1 (530 nm) and FL2 (585 nm) emission channel detectors. Compensation parameters were set at FL1 = 10.5% FL2 and FL2 = 25.9% FL1. Results are presented as a percent of the FL2/FL1 fluorescence intensity ratio of untreated stained cells (100%).

Cell Membrane Integrity. Cells that are undergoing toxicity and cell death lose the ability to control the movement of molecules across their plasma membranes. This can be utilized to study cell death and toxicity by measuring the fluorescence of cells following exposure to the usually cell impairing nucleic acid dye propidium iodide (PI). Cells that fluoresce red on excitation have lost the ability to exclude PI and are therefore thought to be dead or in the act of dying. ECs (100 000) seeded on a 12-well microplate were treated with peptide-coated nanoparticles (1 mL, 3 nM) or DMSO (10%) in 20% HS M199 media for 24 h. After treatment, media was transferred into plastic tubes and cells were harvested from the culture dish with nonenzymatic cell dissociation solution (0.5 mL, Sigma-Aldrich) for 30 min. Harvested cell suspensions were combined with collected media and centrifuged for 5 min at 1500 rpm. Cell pellets were resuspended in HBSS (0.5 mL), and PI stain (20 μL, 0.1 mg/mL, HBSS) was added. Cells were incubated for 10 min on ice prior to measurement of cell-specific fluorescence by flow cytometry (FACSCalibur, BD Biosciences) using a 488 nm excitation wavelength and FL2 (585 nm emission) channel detector. Results were compared to FL2 fluorescence intensity of untreated unstained cells, untreated stained cells, and cells treated with known toxic agents such as high concentrations of DMSO.

Intracellular ROS Levels. Reactive oxygen species are naturally occurring signaling molecules generated inside cells but can also be a marker of cellular stress or activation, with the release of large amounts being related to toxicity. ROS levels in cells were therefore determined using the ROS-specific fluorophore carboxy-H2DFFDA, which shows a green fluorescence when reacted with ROS to form the fluorescent molecule difluorofluorescein (DFF) following exposure to the treatments listed. ECs (100 000) seeded on a 12-well microplate were treated with peptide-coated nanoparticles (1 mL, 3 nM) in 20% HS M199 media for 24 h. After treatment cells were stained with carboxy-H2DFFDA (1 mL, 5 μM in HBSS) for 30 min, and then the media was transferred into plastic tubes and cells were harvested from the culture dish with trypsin/EDTA (0.5 mL, Sigma-Aldrich) for 5 min. Harvested cell suspensions were combined with collected media and centrifuged for 5 min at 1500 rpm. Cell pellets were resuspended in HBSS (0.5 mL). A positive control using hydrogen peroxide (1 mM in HBSS) was added to labeled untreated cells prior to measurements of carboxy-DFF intensity by flow cytometry (FACSCalibur, BD Biosciences) using a 488 nm excitation wavelength and an FL1 (520 nm emission) channel detector. Results were compared to FL1 fluorescence intensity of untreated unstained cells (0%) and hydrogen peroxide treated stained cells (100%).

Quantification of Relative Levels of Angiogenesis-Related Cytokines. The release of pro- and anti-angiogenic factors in the presence and absence of peptide-functionalized nanoparticle treatments was determined using a Proteome profiler kit (R&D). Breast cancer cells (MCF-7 and MDA 100 000 per well) were seeded on 12-well microplates and were treated with the inhibitors (1 mL, 3 nM) in 20% HS M199 media for 24 h. The conditioned media was transferred into plastic tubes and centrifuged for 15 min at 16 400 rpm and 4 °C to remove the nanoparticles and any suspended cells. The supernatant was transferred into new plastic tubes, and the angiogenesis-related cytokines were determined with the Proteome profiler kit (R&D) according to a protocol supplied by the manufacturer. Quantification and analysis of the subsequent dot-blots were performed with ImageJ software, by measuring integral density of spots compared to untreated controls.

Statistical Analysis. One-way ANOVA with Dunnett's post test or two-tailed Student's *t* test was performed using GraphPad

Prism version 5.04 for Windows (GraphPad Software, San Diego, CA, USA) with positive significance shown as $*p < 0.05$, $**p < 0.01$, and $***p < 0.001$, nonsignificant shown as ns, and negative significance shown as $^{\#}p < 0.05$, $^{\#\#}p < 0.01$, and $^{\#\#\#}p < 0.001$.

Conflict of Interest: The authors declare no competing financial interest.

Supporting Information Available: Further experimental details and characterization of nanoparticles. This material is available free of charge *via* the Internet at http://pubs.acs.org.

Acknowledgment. The University of Southampton (NanoUSRG) and Royal Society are gratefully acknowledged for funding of this project. A.G.K. would also like to thank the EU COST actions MP1202, CM1101, and TD1003 for networking opportunities associated with this work. The European Science Foundation is also acknowledged within the framework of the ESF activity PLASMON-BIONANOSENSE. D.B. thanks the School of Physics and Astronomy, EPSRC, for financial support. T.M.M. thanks the EPSRC and AAIR charity for financial support.

REFERENCES AND NOTES

1. Folkman, J.; Shing, Y. Angiogenesis. *J. Biol. Chem.* **1992**, *267*, 10931–10934.
2. Carmeliet, P. Angiogenesis in Health and Disease. *Nat. Med.* **2003**, *9*, 653–660.
3. Carmeliet, P.; Jain, R. K. Angiogenesis in Cancer and Other Diseases. *Nature* **2000**, *407*, 249–257.
4. Folkman, J. Angiogenesis in Cancer, Vascular, Rheumatoid and Other Disease. *Nat. Med.* **1995**, *1*, 27–31.
5. Goodwin, A. M. *In Vitro* Assays of Angiogenesis for Assessment of Angiogenic and Anti-angiogenic Agents. *Microvasc. Res.* **2007**, *74*, 172–183.
6. Risau, W. Mechanisms of Angiogenesis. *Nature* **1997**, *386*, 671–674.
7. D'Andrea, L. D.; Del Gatto, A.; Pedone, C.; Benedetti, E. Peptide-Based Molecules in Angiogenesis. *Chem. Biol. Drug Des.* **2006**, *67*, 115–126.
8. Des Guetz, G.; Uzzan, B.; Chouahnia, K.; Morere, J. F. Cardiovascular Toxicity of Anti-Angiogenic Drugs. *Targ. Oncol.* **2011**, *6*, 197–202.
9. Chung, E.; Ricles, L. M.; Stowers, R. S.; Nam, S. Y.; Emelianov, S. Y.; Suggs, L. J. Multifunctional Nanoscale Strategies for Enhancing and Monitoring Blood Vessel Regeneration. *Nano Today* **2012**, *7*, 514–531.
10. Nichols, J. W.; Bae, Y. H. Odyssey of a Cancer Nanoparticle: From Injection Site to Site of Action. *Nano Today* **2012**, *7*, 606–618.
11. Kievit, F. M.; Zhang, M. Cancer Nanotheranostics: Improving Imaging and Therapy by Targeted Delivery across Biological Barriers. *Adv. Mater.* **2011**, *23*, H217–H247.
12. Banerjee, D.; Harfouche, R.; Sengupta, S. Nanotechnology-Mediated Targeting of Tumor Angiogenesis. *Vasc. Cell* **2011**, *3*, 1–13.
13. Bartczak, D.; Kanaras, A. G. Diacetylene-Containing Ligand as a New Capping Agent for the Preparation of Water-Soluble Colloidal Nanoparticles of Remarkable Stability. *Langmuir* **2010**, *26*, 7072–7077.
14. Charron, G.; Huhn, D.; Perrier, A.; Cordier, L.; Pickett, C. J.; Nan, T.; Parak, W. J. On the Use of pH Titration to Quantitatively Characterize Colloidal Nanoparticles. *Langmuir* **2012**, *28*, 15141–15149.
15. Conde, J.; Ambrosone, A.; Sanz, V.; Hernandez, Y.; Marchesano, V.; Tian, F. R.; Child, H.; Berry, C. C.; Ibarra, M. R.; Baptista, P. V.; *et al*. Design of Multifunctional Gold Nanoparticles for *in Vitro* and *in Vivo* Gene Silencing. *ACS Nano* **2012**, *6*, 8316–8324.
16. Quarta, A.; Curcio, A.; Kakwere, H.; Pellegrino, T. Polymer Coated Inorganic Nanoparticles: Tailoring the Nanocrystal Surface for Designing Nanoprobes with Biological Implications. *Nanoscale* **2012**, *4*, 3319–3334.
17. Thanh, N. T. K.; Green, L. A. W. Functionalization of Nanoparticles for Biomedical Applications. *Nano Today* **2010**, *5*, 213–230.
18. Lu, Z.; Yin, Y. Colloidal Nanoparticle Clusters: Functional Materials by Design. *Chem. Soc. Rev.* **2012**, *41*, 6874–6887.
19. Fairbairn, N.; Christofidou, A.; Kanaras, A. G; Muskens, O. L. Hyperspectral Darkfield Microscopy of Single Hollow Gold Nanoparticles for Biomedical Applications. *Phys. Chem. Chem. Phys.* **2013**, *15*, 4163–4168.
20. Arvizo, R. R.; Bhattacharyya, S.; Kudgus, R. A.; Giri, K.; Bhattacharya, R.; Mukherjee, P. Intrinsic Therapeutic Applications of Noble Metal Nanoparticles: Past, Present, Future. *Chem. Soc. Rev.* **2012**, *41*, 2943–2970.
21. Dreaden, E. C.; Alikilany, M. A.; Huang, X.; Murphy, C. J.; El-Sayed, M. A. The Golden Age: Gold Nanoparticles in Biomedicine. *Chem. Soc. Rev.* **2012**, *41*, 2740–2779.
22. Rosman, C.; Pierrat, S.; Henkel, A.; Tarantola, M.; Schneider, D.; Sunnick, E.; Janshoff, A.; Sönnichsen, C. A New Approach to Assess Gold Nanoparticle Uptake by Mammalian Cells: Combining Optical Dark-Field and Transmission Electron Microscopy. *Small* **2012**, *8*, 3683–3690.
23. Rodríguez-Lorenzo, L.; Krpetic, Z.; Barbosa, S.; Alvarez-Puebla, R. A.; Liz-Marzán, L. M.; Prior, I. A.; Brust, M. Intracellular Mapping with SERS-Encoded Gold Nanostars. *Integr. Biol.* **2011**, *9*, 922–926.
24. Halas, N. J.; Lal, S.; Chang, W. S.; Link, S.; Nordlander, P. Plasmons in Strongly Coupled Metallic Nanostructures. *Chem. Rev.* **2011**, *111*, 3913–3961.
25. Bhattacharya, R.; Mukherjee, P. Biological Properties of "Naked" Metal Nanoparticles. *Adv. Drug Delivery Rev.* **2008**, *60*, 1289–1306.
26. Kim, J. H.; Kim, M. H.; Yu, Y. S.; Lee, T. G. The Inhibition of Retinal Neovascularization by Gold Nanoparticles *via* Suppression of VEGFR-2 Activation. *Biomaterials* **2011**, *32*, 1865–1871.
27. Patra, C. R.; Moneim, S. S. A.; Wang, E.; Dutta, S.; Patra, S.; Eshed, M.; Mukherjee, P.; Gedanken, A.; Shah, V. H.; Mukhopadhyay, D. *In Vivo* Toxicity Studies of Europium Hydroxide Nanorods in Mice. *Toxicol. Appl. Pharmacol.* **2009**, *249*, 88–98.
28. Patra, C. R.; Bjattacharya, R.; Patra, S.; Vlahakis, N. E.; Gabashvili, A.; Koltypin, Y.; Gedanken, A.; Mukherjee, P.; Mukhopadhyay, D. Pro-Angiogenic Properties of Europium (III) Hydroxide Nanorods. *Adv. Mater.* **2008**, *20*, 753–756.
29. Mukherjee, P.; Bhattacharya, R.; Wang, P.; Wang, L.; Basu, S.; Nagy, J. A.; Atala, A.; Mukhopadhyay, D.; Soker, S. Antiangiogenic Properties of Gold Nanoparticles. *Clin. Cancer Res.* **2005**, *11*, 3530–3534.
30. Bhattacharya, R.; Mukherjee, P.; Xiong, Z.; Atala, A.; Soker, S. Mukhopadhyay Gold Nanoparticles Inhibit VEGF165-Induced Proliferation of HUVEC Cells. *Nano Lett.* **2004**, *4*, 2479–2481.
31. Arvizo, R. R.; Rana, S.; Miranda, O. R.; Bhattacharya, R.; Rotello, V. M.; Mukherjee, P. Mechanism of Anti-Angiogenic Property of Gold Nanoparticles: Role of Nanoparticle Size and Surface Charge. *Nanomed.: Nanotechnol., Biol., Med.* **2011**, *7*, 580–587.
32. Bartczak, D.; Nitti, S.; Millar, T. M.; Kanaras, A. G. Exocytosis of Peptide Functionalized Gold Nanoparticles in Endothelial Cells. *Nanoscale* **2012**, *4*, 4470–4472.
33. Bartczak, D.; Muskens, O. L.; Nitti, S.; Millar, T. M.; Sanchez-Elsner, T.; Kanaras, A. G. Interactions of Human Endothelial Cells with Gold Nanoparticles of Different Morphologies. *Small* **2012**, *8*, 122–130.
34. Bartczak, D.; Muskens, O. L.; Millar, T. M.; Sanchez-Elsner, T.; Kanaras, A. G. Laser-Induced Damage and Recovery of Plasmonically Targeted Human Endothelial Cells. *Nano Lett.* **2011**, *11*, 1358–1363.
35. Bartczak, D.; Sanchez-Elsner, T.; Louafi, F.; Millar, T. M.; Kanaras, A. G. Receptor-Mediated Interactions between Colloidal Gold Nanoparticles and Human Umbilical Vein Endothelial Cells. *Small* **2011**, *7*, 388–394.
36. Turkevich, J.; Stevenson, P. C.; Hillier, J. A Study of the Nucleation and Growth Processes in the Synthesis of Colloidal Gold. *Discuss. Faraday Soc.* **1951**, *11*, 55–75.
37. Kanaras, A. G.; Kamounah, F. S.; Schaumburg, K.; Kiely, C.; Brust, M. Thioalkylated Tetraethylene Glycol: A New Ligand

for Water Soluble Monolayer Protected Gold Clusters. *Chem. Commun.* **2002**, *20*, 2294–2295.
38. Bartczak, D.; Kanaras, A. G. Preparation of Peptide Functionalized Gold Nanoparticles Using One Pot EDC/sulfo-NHS Coupling. *Langmuir* **2011**, *27*, 10119–10123.
39. Niemisto, A.; Dunmire, V.; Yli-Harja, O.; Zhang, W.; Shmulevich, I. Robust Quantification of *in Vitro* Angiogenesis through Image Analysis. *IEEE Trans. Med. Imaging* **2005**, *24*, 549–553.
40. Neufeld, G.; Cohen, T.; Gengrinovitch, S.; Poltorak, Z. Vascular Endothelial Growth Factor (VEGF) and its Receptors. *FASEB J.* **1999**, *13*, 9–22.
41. Murga, M.; Fernandez-Capetillo, O.; Tosato, G. Neuropilin-1 Regulates Attachment in Human Endothelial Cells Independently of Vascular Endothelial Growth Factor Receptor-2. *Blood* **2005**, *105*, 1992–1999.
42. Clauss, M.; Breier, G. *Mechanisms of Angiogenesis*; Brikhauser Verlag: Basel, 2005.